

1 **Multi-trait random regression models**
2 **increase genomic prediction accuracy for a**
3 **temporal physiological trait derived from**
4 **high-throughput phenotyping**

5 Toshihi Baba¹, Mehdi Momen¹, Malachy T. Campbell¹, Harkamal Walia²,
6 and Gota Morota^{1*}

7 ¹Department of Animal and Poultry Sciences, Virginia Polytechnic Institute
8 and State University, Blacksburg, VA, USA 24061

9 ²Department of Agronomy and Horticulture, University of Nebraska,
10 Lincoln, NE 68583

11 Keywords: Genomic correlation, Genomic prediction, High-throughput phenotyping, Longi-
12 tudinal trait, Random regression model

13

14 Running title: Multi-trait longitudinal genetic analysis

15

16 ORCID: 0000-0002-6637-2056 (TB), 0000-0002-2562-2741 (MM), 0000-0002-8257-3595 (MTC),
17 0000-0002-9712-5824 (HW), and 0000-0002-3567-6911 (GM).

18

19 * Corresponding author:

20

21 Gota Morota

22 Department of Animal and Poultry Sciences

23 Translational Plant Sciences Program

24 175 West Campus Drive

25 Blacksburg, Virginia 24061 USA.

26 Virginia Polytechnic Institute and State University

27 E-mail: morota@vt.edu

28

29 Abstract

30 Random regression models (RRM) are used extensively for genomic inference and prediction
31 of time-valued traits in animal breeding, but only recently have been used in plant systems.
32 High-throughput phenotyping (HTP) platforms provide a powerful means to collect high-
33 dimensional phenotypes throughout the growing season for large populations. However, to
34 date, selection of an appropriate statistical genomic framework to integrate multiple temporal
35 traits for genomic prediction in plants remains unexplored. Here, we demonstrate the utility
36 of a multi-trait RRM (MT-RRM) for genomic prediction of daily water usage (WU) in rice
37 (*Oryza sativa*) through joint modeling with shoot biomass (projected shoot area, PSA).
38 Three hundred and fifty-seven accessions were phenotyped daily for WU and PSA over 20
39 days using a greenhouse-based HTP platform. MT-RRMs that modeled additive genetic
40 and permanent environmental effects for both traits using quadratic Legendre polynomials
41 were used to assess genomic correlations between traits and genomic prediction for WU.
42 Predictive abilities of the MT-RRMs were assessed using two cross-validation (CV) scenarios.
43 The first scenario was designed to predict genetic values for WU at all time points for a set
44 of accessions with unobserved WU. The second scenario was designed to forecast future
45 genetic values for WU for a panel of known accessions with records for WU at earlier time
46 periods. In each scenario we evaluated two MT-RRMs in which PSA records were absent or
47 available for time points in the testing population. Moderate to strong genomic correlations
48 between WU and PSA were observed across the days of imaging (0.29-0.87). In both CV
49 scenarios, MT-RRMs showed better predictive abilities compared to single-trait RRM, and
50 prediction accuracies were greatly improved when PSA records were available for the testing
51 population. In summary, these frameworks provide an effective approach to predict temporal
52 physiological traits that are difficult or expensive to quantify in large populations.

53 Background

54 High-throughput phenotyping (HTP) is an innovative tool in plant breeding. HTP pro-
55 vides precise and non-destructive estimation of multiple complex traits that describe growth
56 and development (e.g., height, biomass, and flowering time) or environmental responses
57 (e.g., chlorophyll fluorescence, canopy temperature, and water content) using non-destructive
58 image-based phenotyping (Araus et al., 2018; Morota et al., 2019). These HTP data mitigate
59 extensive costs associated with manual phenotyping, and can be used to better capture the
60 plant’s phenome. In the context of plant breeding and genetics, these data can be used to
61 improve the prediction of breeding values for a target trait of interest, thereby improving
62 the accuracy of selection, as well as provide insights into how secondary traits influence a
63 trait of interest (Araus et al., 2018; Morota et al., 2019; Voss-Fels et al., 2019).

64 For many genome-enabled breeding programs, developing phenotyping and statistical
65 approaches to improve prediction of breeding values and accelerate selection is the primary
66 objective (Campbell et al., 2018; Juliana et al., 2019; Voss-Fels et al., 2019). In many breed-
67 ing programs, the agronomic value of breeding materials is evaluated using multiple traits.
68 These traits are often correlated at the genetic level. One standard approach for predicting
69 breeding values is to jointly fit all phenotypes in a single model using a multi-trait (MT)
70 approaches (Kadarmideen et al., 2003). These approaches capture the genetic covariances
71 between traits, and have been shown to improve the prediction of breeding values compared
72 to single trait approaches for phenotypes with limited records or low heritability (Calus and
73 Veerkamp, 2011; Jia and Jannink, 2012; Guo et al., 2014). Thus, the MT framework can be
74 particularly advantageous when the target trait has low heritability, but is correlated with
75 a more heritable trait; or when the trait of interest is difficult or costly to evaluate and
76 only incomplete data can be collected, and the trait of interest is correlated with a trait
77 that is easier and cheaper to evaluate. Thus, in the context of HTP, MT genomic predic-
78 tion approaches can accommodate the high-dimensional multi-trait data generated by these
79 platforms. Moreover, secondary phenotypes recorded with HTP can be included in the pre-

80 diction framework to improve prediction of a target trait such as yield. These applications
81 have been shown in a recent study by (Sun et al., 2017).

82 While several studies have highlighted the advantages of MT frameworks for genomic
83 prediction, HTP-derived MT data often introduce an additional level of complexity-the time
84 axis. The standard MT framework may not be appropriate in cases where multiple pheno-
85 types are recorded at regular intervals throughout the growing season or for the duration
86 of the experiment. While MT frameworks can be fit to these data, the assumptions of the
87 MT framework bring to question whether the conventional MT model should be used. For
88 instance, one assumption is that each phenotype in the MT model is finite characteristic
89 (Kirkpatrick et al., 1990). While this is certainly true for two phenotypes such as yield or
90 protein content, this is certainly not the case for a phenotype recorded at two time points
91 (Kirkpatrick et al., 1990). Temporal phenotypes are infinite-dimensional traits, meaning
92 that although there are only records for discrete time intervals, we expect that the pheno-
93 type will vary continuously with time between the two intervals. With these data, a more
94 appropriate solution is to treat the temporal phenotypes as continuous characteristics and
95 perform genetic analyses using random regression models (RRM).

96 RRM model the covariance between time points as a continuous function of time (Mrode,
97 2014). While several covariance functions can be utilized, Legendre polynomials or B-splines
98 are routinely used . The use of orthogonal Legendre polynomials in RRM offers numeri-
99 cal stability by reducing correlation between random regression coefficients and computing
100 error (Schaeffer, 2004). With RRM, temporal phenotypes are partitioned into genetic, per-
101 manent environmental effects, and residuals (Mrode, 2014). With repeated measurements,
102 it is assumed that there is additional resemblance between records of an individual due to
103 environmental factors or circumstances that affect the records of the individual permanently
104 (Mrode, 2014). Thus, the random permanent environment term captures this non-genetic
105 resemblance between time points. Covariance functions are used to model both genetic
106 and permanent environmental effects (Kirkpatrick et al., 1990; Schaeffer and Dekkers, 1994;

107 Meyer and Hill, 1997; Schaeffer, 2004). Thus, the RRM prediction framework provides so-
108 lutions for random regression coefficients for random effects. Given coefficients for random
109 genetic effects, the genetic values at any time point can be easily calculated. Recently,
110 RRM have been used for genomic analyses of longitudinal image-based HTP traits in plants
111 (Campbell et al., 2018, 2019; Momen et al., 2019a). The ability of these frameworks to
112 forecast future phenotypes using the records at earlier time has been shown by Campbell
113 et al. (2018) and Momen et al. (2019a) based on a digital metric for shoot biomass, known
114 as projected shoot area (PSA). PSA is a digital metric derived from images taken of each
115 plant and is highly correlated with destructive measures of shoot biomass (Golzarian et al.,
116 2011; Berger et al., 2010; Campbell et al., 2015).

117 However, given the capability of HTP to collect multiple temporal phenotypes, one un-
118 resolved question in plant breeding is how to jointly model multiple temporal phenotypes.
119 To address this, we aimed to integrate the RRM framework for temporal traits into a MT
120 model. We utilized a data set in which PSA and water use (WU) was recorded daily over
121 a period of 20 days. The aim of the study was to evaluate the ability of multi-trait ran-
122 dom regression model (MT-RRM) and a single-trait random regression model (ST-RRM) to
123 predict WU by borrowing information from PSA. The rationale is that WU is much more
124 difficult to evaluate in most studies compared to PSA and is likely to be more influenced
125 by environmental effects, and thus have lower heritability compared to shoot biomass. The
126 models were compared using several cross-validation (CV) scenarios.

127 **Materials and Methods**

128 **Plant materials and greenhouse conditions**

129 This study utilized HTP records from 378 of the 432 accessions of rice (*Oryza sativa*) diversity
130 panel 1 (RDP1) (Zhao et al., 2011). Sixty four accessions were excluded due to lack of seed
131 availability or poor germination. Seeds were treated with Thiram fungicide and germinated
132 on moist paper towels in plastic boxes for three days. Three uniformly germinated seedlings
133 were selected for each accession and transplanted to pots (150mm diameter x 200 mm height)
134 filled with 2.5 kg of UC Mix. The plants were grown in saturated soil on greenhouse benches
135 prior to phenotyping.

136 Plants were thinned to one seedling per pot seven days after transplant (DAT), and two
137 layers of blue mesh were placed on top of the pots to reduce evaporation. The plants were
138 loaded on to the imaging system at 13 DAT. The automated phenotyping system was set
139 to maintain all plants at 90% field capacity. The experiment followed a partially replicated
140 design (Cullis et al., 2006). The p-rep design was modified to accommodate the two water
141 treatments (control and drought conditions) and allow comparison of treatments within each
142 accession. Each accession was assigned to two consecutive pots, and the water treatments
143 were randomly assigned to each pot. Each experiment consisted of 378 accessions from RDP1
144 and was repeated three times from February to April 2016. The accessions were distributed
145 across 432 pots positioned across 24 lanes (18 plants/pots in each lane). These 432 pots
146 belonged to 378 accessions, of which 54 had more than one replicate in each experiment.
147 The same 54 accessions were replicated twice in each experiment. Of these 378 accessions,
148 357 accessions had genotypic data. All experiments were conducted at the Plant Accelerator
149 Australian Plant Phenomics Facility, at the University of Adelaide, SA, Australia.

150 Phenotypic data

151 Beginning at 13 DAT all plants were phenotyped daily for shoot biomass and WU using the
152 automated greenhouse system, and each plant was imaged daily over a period of 20 days
153 using a visible (red-green-blue / RGB) camera (Basler Pilot piA240012 gc, Ahrensburg,
154 Germany). For each plant, three images were taken in each recording day: two side-view
155 angles separated by 90 degree and a single top view. Plant pixels were extracted from RGB
156 images using the LemnaGrid software, and the plant pixels from the three images were
157 summed to obtain a digital measure of shoot biomass. We refer to this metric as PSA.
158 Several studies have shown this to be an accurate proxy for shoot biomass (Golzarian et al.,
159 2011; Campbell et al., 2015; Knecht et al., 2016).

160 After imaging, each plant was watered to a predefined weight to maintain 90% field
161 capacity. The automated watering system collects the start weight, final weight and amount
162 of water that was added for each pot. Thus, from these data we can estimate the amount of
163 water that lost by evapotranspiration each day. WU was calculated as $WU_t = Potwt_{t-1} -$
164 $Potwt_t$. Where $Potwt_{t-1}$ is the weight of the pot after watering on the previous day, and
165 $Potwt_t$ is the weight of the pot on the current day prior to watering (Momen et al., 2019b).

In this study, we used observations collected in the control condition. Best linear unbiased estimators (BLUE) were obtained for each accession and day using the following model

$$y_{ijkn} = \mu + A_i + E_{jk} + B_{jkn} + AE_{ij} + e_{ijkn}$$

166 where μ is the overall mean, A_i is the effect of the i^{th} accession, E_{jk} is the effect of the j^{th}
167 experiment in the k^{th} replicate, B_{jkn} is the block effect of the n^{th} smart house in the j^{th}
168 experiment and the k^{th} replicate, AE_{ij} is the interaction of accession and experiment. All
169 the effects, except A_i were considered random.

170 Genotypic data

171 All accessions were genotyped with a 44,000 single nucleotide polymorphisms (SNPs) array
172 (Zhao et al., 2011). Genotypic data regarding the rice accessions can be downloaded from the
173 rice diversity panel website (<http://www.ricediversity.org/>). SNPs with call rate ≤ 0.95 and
174 minor allele frequency ≤ 0.05 were removed. Missing genotypes were imputed using Beagle
175 software version 3.3.2 (Browning and Browning, 2007) following Momen et al. (2019b). A
176 total of 34,993 SNPs remained for downstream analyses.

177 Single-trait random regression model

Campbell et al. (2018) and Momen et al. (2019a) have applied ST-RRM for PSA. In this study, a similar statistical model was used to model WU. The model is given by

$$y_{jt} = \sum_{k=0}^2 \phi(t)_{jk} b_k + \sum_{k=0}^2 \phi(t)_{jk} u_{jk} + \sum_{k=0}^2 \phi(t)_{jk} p_{jk} + e_{jt},$$

where y_{jt} is the BLUE of j th accession for WU at time point t , b_k is the k th fixed Legendre regression coefficients for overall mean, u_{jk} is the k th random regression coefficients for additive genetic effect, p_{jk} is the k th random regression coefficients for permanent environmental effect, e_{jt} is the vector of residuals, and $\phi(t)_{jk}$ is a time covariate coefficient defined by a k th Legendre polynomial evaluated at time point t belonging to the j th accession. The permanent environmental effect captures constant environmental factors that affect the successive records of an accession throughout the time course (Mrode, 2014). We set quadratic Legendre polynomials of all the effects, based on the results of Momen et al. (2019a) which investigated the prediction accuracy of PSA using ST-RRM. The first order of the Legendre polynomial (i.e., an intercept) was standardized to 1 (Gengler et al., 1999). In matrix notation, the model is given by

$$\mathbf{y} = \mathbf{Xb} + \mathbf{Zu} + \mathbf{Qp} + \mathbf{e},$$

where \mathbf{y} is the vector of observations for WU, \mathbf{b} is the vector of fixed effect, \mathbf{u} is the vector of random additive genetic effect, \mathbf{p} is the vector of random permanent environmental effect, \mathbf{e} is the vector of random residual effect, and \mathbf{X} , \mathbf{Z} , and \mathbf{Q} are corresponding incidence matrices. The covariance structures were defined as the following.

$$\text{Var} \begin{bmatrix} \mathbf{u} \\ \mathbf{p} \\ \mathbf{e} \end{bmatrix} = \begin{bmatrix} \mathbf{C} \otimes \mathbf{G} & \mathbf{0} & \mathbf{0} \\ \mathbf{0} & \mathbf{D} \otimes \mathbf{I} & \mathbf{0} \\ \mathbf{0} & \mathbf{0} & \mathbf{I} \otimes \mathbf{R} \end{bmatrix},$$

where \mathbf{G} is a genomic relationship matrix calculated by $\mathbf{W}\mathbf{W}'/m$ according to VanRaden (2008), \mathbf{W} is a centered and scaled matrix, m is the number of SNPs, \mathbf{I} is an identity matrix, \mathbf{C} and \mathbf{D} are covariance matrices of additive genetic and permanent environmental effects, \mathbf{R} is a diagonal matrix of heterogeneous residual variance at each time period, and \otimes is the Kronecker product. The covariance matrices \mathbf{C} and \mathbf{D} are defined as follows.

$$\mathbf{C} = \begin{bmatrix} v_u^0 & v_u^{01} & v_u^{02} \\ v_u^{10} & v_u^1 & v_u^{12} \\ v_u^{20} & v_u^{21} & v_u^2 \end{bmatrix}, \quad \mathbf{D} = \begin{bmatrix} v_p^0 & v_p^{01} & v_p^{02} \\ v_p^{10} & v_p^1 & v_p^{12} \\ v_p^{20} & v_p^{21} & v_p^2 \end{bmatrix},$$

178 where v_u^k and v_p^k are the variance components of k th order random regression coefficients
 179 for additive genetic and permanent environment effects, respectively, and v_u^{kl} and v_p^{kl} are the
 180 covariances between k th and l th order random regression coefficients for additive genetic and
 181 permanent environmental effects, respectively.

182 Multi-trait random regression model

For MT-RRM, the ST-RRM for WU described above is expanded to include PSA information as follows.

$$\begin{bmatrix} \mathbf{y}_1 \\ \mathbf{y}_2 \end{bmatrix} = \begin{bmatrix} \mathbf{X}_1 & \mathbf{0} \\ \mathbf{0} & \mathbf{X}_2 \end{bmatrix} \begin{bmatrix} \mathbf{b}_1 \\ \mathbf{b}_2 \end{bmatrix} + \begin{bmatrix} \mathbf{Z}_1 & \mathbf{0} \\ \mathbf{0} & \mathbf{Z}_2 \end{bmatrix} \begin{bmatrix} \mathbf{u}_1 \\ \mathbf{u}_2 \end{bmatrix} + \begin{bmatrix} \mathbf{Q}_1 & \mathbf{0} \\ \mathbf{0} & \mathbf{Q}_2 \end{bmatrix} \begin{bmatrix} \mathbf{p}_1 \\ \mathbf{p}_2 \end{bmatrix} + \begin{bmatrix} \mathbf{e}_1 \\ \mathbf{e}_2 \end{bmatrix},$$

where subscripts 1 and 2 refer to WU and PSA, respectively. The covariance structures of \mathbf{C} and \mathbf{D} were also expanded as follows.

$$\mathbf{C} = \begin{bmatrix} \mathbf{C}_1 & \mathbf{C}_{12} \\ \mathbf{C}_{12}^T & \mathbf{C}_2 \end{bmatrix}, \quad \mathbf{D} = \begin{bmatrix} \mathbf{D}_1 & \mathbf{D}_{12} \\ \mathbf{D}_{12}^T & \mathbf{D}_2 \end{bmatrix}$$

183 where \mathbf{C}_1 and \mathbf{C}_2 (\mathbf{D}_1 and \mathbf{D}_2) are 3×3 variance-covariance submatrices of random regression
 184 coefficients for each trait and \mathbf{C}_{12} (\mathbf{D}_{12}) is a 3×3 covariance submatrix of random regression
 185 coefficients between the traits. Thus, the whole \mathbf{C} and \mathbf{D} matrices take the form

$$\mathbf{C} = \begin{bmatrix} v_{u_1}^0 & v_{u_1}^{01} & v_{u_1}^{02} & v_{u_{12}}^{00} & v_{u_{12}}^{01} & v_{u_{12}}^{02} \\ v_{u_1}^{10} & v_{u_1}^1 & v_{u_1}^{12} & v_{u_{12}}^{10} & v_{u_{12}}^{11} & v_{u_{12}}^{12} \\ v_{u_1}^{20} & v_{u_1}^{21} & v_{u_1}^2 & v_{u_{12}}^{20} & v_{u_{12}}^{21} & v_{u_{12}}^{22} \\ v_{u_{21}}^{00} & v_{u_{21}}^{10} & v_{u_{21}}^{20} & v_{u_2}^0 & v_{u_2}^{01} & v_{u_2}^{02} \\ v_{u_{21}}^{10} & v_{u_{21}}^{11} & v_{u_{21}}^{21} & v_{u_2}^{10} & v_{u_2}^1 & v_{u_2}^{12} \\ v_{u_{21}}^{20} & v_{u_{21}}^{21} & v_{u_{21}}^{22} & v_{u_2}^{20} & v_{u_2}^{21} & v_{u_2}^2 \end{bmatrix}, \quad \mathbf{D} = \begin{bmatrix} v_{p_1}^0 & v_{p_1}^{01} & v_{p_1}^{02} & v_{p_{12}}^{00} & v_{p_{12}}^{01} & v_{p_{12}}^{02} \\ v_{p_1}^{10} & v_{p_1}^1 & v_{p_1}^{12} & v_{p_{12}}^{10} & v_{p_{12}}^{11} & v_{p_{12}}^{12} \\ v_{p_1}^{20} & v_{p_1}^{21} & v_{p_1}^2 & v_{p_{12}}^{20} & v_{p_{12}}^{21} & v_{p_{12}}^{22} \\ v_{p_{21}}^{00} & v_{p_{21}}^{10} & v_{p_{21}}^{20} & v_{p_2}^0 & v_{p_2}^{01} & v_{p_2}^{02} \\ v_{p_{21}}^{10} & v_{p_{21}}^{11} & v_{p_{21}}^{21} & v_{p_2}^{10} & v_{p_2}^1 & v_{p_2}^{12} \\ v_{p_{21}}^{20} & v_{p_{21}}^{21} & v_{p_{21}}^{22} & v_{p_2}^{20} & v_{p_2}^{21} & v_{p_2}^2 \end{bmatrix},$$

where $v_{u_1}^k$ and $v_{p_1}^k$ ($v_{u_2}^k$ and $v_{p_2}^k$) are variance components of k th order random regression coefficients for additive genetic and permanent environment terms for WU (PSA), $v_{u_1}^{kl}$ and $v_{p_1}^{kl}$ ($v_{u_2}^{kl}$ and $v_{p_2}^{kl}$) are covariances between k th and l th order random regression coefficients for additive genetic or permanent environmental effects within WU (PSA), and $v_{u_{12}}^{kl}$ and $v_{p_{12}}^{kl}$ are

covariances between k th and l th order random regression coefficients for additive genetic and permanent environmental effects between WU and PSA, respectively. As with ST-RRM, we assumed the residual variance for each day of imaging was unique. Thus, a heterogeneous residual variance structure was used for MT-RRM. The matrix of residual variance at time t ($\mathbf{R}_{(t)}^*$) is presented as:

$$\mathbf{R}_{(t)}^* = \begin{bmatrix} v_{e_{1(t)}} & v_{e_{12(t)}} \\ v_{e_{21(t)}} & v_{e_{2(t)}} \end{bmatrix}$$

186 where $v_{e_{1(t)}}$ and $v_{e_{2(t)}}$ are residual variances for WU and PSA, respectively, and $v_{e_{12(t)}}$ ($v_{e_{21(t)}}$)
187 is the residual covariance between WU and PSA at time point t .

188 Estimation of genomic correlation at each time point

Genomic correlation between WU and PSA at each time point from MT-RRM was computed as follows.

$$\frac{\mathbf{t}_i \mathbf{C}_{12} \mathbf{t}_i'}{\sqrt{\mathbf{t}_i \mathbf{C}_1 \mathbf{t}_i'} \sqrt{\mathbf{t}_i \mathbf{C}_2 \mathbf{t}_i'}}$$

189 where $\mathbf{t}_i = \phi_{ik}$ is the i th row vector of the 20×3 basis function matrix (Φ) with the
190 k th order of fit (Mrode, 2014). Here, Φ is given as $\mathbf{M}\mathbf{A}$, where \mathbf{M} is a matrix of second
191 order polynomials of standardized time values and \mathbf{A} is a matrix of coefficients for a second
192 order Legendre polynomial (Kirkpatrick et al., 1990). We used the GIBBS3F90 program to
193 estimate genetic parameters (Misztal et al., 2002). The GIBBS3F90 program solves mixed
194 model equations in the Bayesian framework by assuming heterogeneous residual variances.

195 Cross-validation scenarios

196 We investigated the prediction performance of genetic values for WU from RRM using two
197 CV scenarios as shown in Figure 1. For each CV scenario, we compared three models as
198 described below.

199 **CV1:** The objective of this scenario was to assess the ability of ST-RRM and MT-RRM to

200 predict WU for a set of new accessions without records on WU. To this end, the accessions
201 were split into testing and training sets with 245 accessions allocated to the training set and
202 112 allocated to the testing set. First, we fitted ST-RRM using genomic and phenotypic
203 data on the training subset and the genetic values of WU were predicted for all accessions
204 in the testing set. This ST-RRM served as a baseline to evaluate MT-RRM. We evaluated
205 two different types for MT-RRM. The first MT-RRM (MT-RRM1) can be thought of as
206 a conventional genomic prediction application in which a model is fitted using a training
207 population that has genomic data and phenotypic records for both traits. This model is
208 used to predict genomic values for WU in a testing population that has genotypic data, but
209 no records for either trait. In the second MT-RRM (MT-RRM2), complete PSA and WU
210 records were available for the training population, while only PSA phenotypes were available
211 for the testing population. The rationale for this scenario is that it is often much easier to
212 obtain non-destructive measurements for shoot biomass compared to WU. Thus, this can be
213 thought of as a case in which a portion of the population has incomplete data.

214 Genetic values of testing individuals for WU at time t from ST-RRM and MT-RRM1
215 were calculated by $\hat{\mathbf{a}}_{\text{tst}}^t = \mathbf{G}_{\text{tst},\text{trn}} \mathbf{G}_{\text{trn},\text{trn}}^{-1} \hat{\mathbf{a}}_{\text{trn}}^t$, where $\mathbf{G}_{\text{tst},\text{trn}}$ is the genomic relationship matrix
216 between testing and training individuals, $\mathbf{G}_{\text{trn},\text{trn}}^{-1}$ is the inverse of genomic relationship matrix
217 of training individuals, and $\hat{\mathbf{a}}_{\text{trn}}^t = \mathbf{\Phi} \hat{\mathbf{u}}_{1,\text{trn}}$ is the vector of genetic values at time t (Momen
218 et al., 2019a). On the other hand, the genetic values of testing individuals for WU from
219 MT-RRM2 can be directly obtained from best linear unbiased prediction (BLUP) solutions
220 because the model included the genomic relationship matrix of all accessions by fitting PSA
221 phenotypes for the testing individuals. Thus, the genetic values of WU for the testing
222 individuals at time t were computed by $\hat{\mathbf{a}}_{\text{tst}}^t = \mathbf{\Phi} \hat{\mathbf{u}}_{1,\text{trn}}$.

223 **CV2:** This cross-validation was designed to evaluate the ability of the MT-RRM and ST-
224 RRM to predict genetic values of WU at future time points. Thus, it can be thought of as a
225 forecasting approach. The training dataset consisted of phenotypic records for 245 randomly
226 selected for the first 10 days of imaging. The models were used to predict genetic values for

227 days 11 to 20. As with the first scenario, we assessed their genomic predictions by using
228 ST-RRM and two kinds of MT-RRM from the training data. MT-RRM1 used records of
229 WU and PSA from day 1 to day 10 of imaging as training data, while MT-RRM2 used WU
230 records from the first 10 days of imaging and PSA values from 1 to 20 to train the model.
231 We computed the genetic values of WU at day 11 to 20 as $\Phi_{11:20}\hat{\mathbf{u}}_{1,\text{trn}}$ where $\Phi_{11:20}$ is the
232 basis function matrix at 11 to 20 days and $\hat{\mathbf{u}}_{1,\text{trn}}$ is the vector of random additive genetic
233 effect for WU of testing individuals.

234 To assess prediction accuracy, Pearson correlation was calculated between predicted ge-
235 netic values and BLUE of WU at each time point in the testing population. Each CV
236 scenario was repeated 10 times. We used the GIBBS3F90 program with a fixed variance
237 option to perform genomic prediction in all the CV scenarios. We estimated variance com-
238 ponents in the training set and genetic values were predicted in the testing set condition on
239 the estimated variance components.

240 Results

241 Assessing temporal water use and shoot biomass trajectories in rice

242 To assess the temporal relationships between shoot biomass production and WU, a panel of
243 357 rice accessions was phenotyped over a period of 20 days using a non-destructive image-
244 based phenotyping platform. This system provides a means to non-destructively assess
245 plant growth and morphology, and allows WU to be assessed throughout the duration of the
246 experiment (Berger et al., 2010; Campbell et al., 2015; Fahlgren et al., 2015; Feldman et al.,
247 2018).

248 Figure 2 shows a boxplot of the BLUE after an adjustment by fixed effects for WU over
249 20 time days of imaging. WU exhibited an exponential trend over the 20 days of imaging
250 and closely followed the temporal patterns exhibited by PSA.

251 Joint analysis of WU and PSA reveals shared additive genetic ef- 252 fects between traits

253 Genetic architectures of WU and PSA were dissected by estimating the proportion of cap-
254 tured additive genetic variances across 20 days of imaging using a ST-RRM. The RRM
255 included a fixed second order Legendre polynomial to capture the overall mean trajectories
256 for each trait, and additive genetic and permanent environmental effects were modeled us-
257 ing a second order Legendre polynomial. Figure 3 shows that PSA exhibited considerably
258 higher narrow-sense heritability (h^2) compared to WU. For instance, h^2 ranged from 0.48 to
259 0.82 for PSA, while the values ranged from 0.20 to 0.73 for WU. We observed an increasing
260 trend over time with the lowest value observed on day 1 of imaging and the highest value
261 observed on day 19. PSA on the other hand showed the lowest h^2 values on day 1, but it
262 quickly increased and reached somewhat of a plateau from day 3 to 16. After day 16, h^2
263 slowly declined. Collectively, these results indicate that both traits are influenced by addi-
264 tive genetic effects, and these effects vary throughout time. However, phenotypic variance is

265 less influenced by non-genetic effects for PSA compared to WU. Moreover, additive genetic
266 effects for WU show greater temporal variability compared to PSA.

267 To investigate genetic relationship between WU and PSA, we estimated genomic correla-
268 tion at each time point. The MT-RRM used a second order polynomial to model the overall
269 mean trends for each trait, as well as the additive genetic and permanent environmental
270 effects for both traits. The genomic correlation between WU and PSA from MT-RRM is
271 shown in Figure 4. A moderate to strong positive genomic correlation between WU and
272 PSA was observed over 20 time periods. On average, the genomic correlation across all
273 time periods was 0.78. The genomic correlation was low for the first time point, but quickly
274 increased until the fifth day of imaging. From day 5 to the final day of imaging, genomic
275 correlation showed a slight increasing trend. Genomic correlation ranged from 0.29 to 0.87,
276 with the highest value observed on the last 12 days of imaging. These results indicate that
277 WU and PSA share similarity at the genetic level.

278 **Predictive assessment using RRM by two CV scenarios**

279 We next sought to evaluate the predictive performance of MT-RRM to predict genetic values
280 for WU. To this end, we employed two CV scenarios. The first is similar to a conventional
281 genomic prediction application in which the objective is to predict genetic values for a set
282 of individuals without phenotypic records. We used two different testing populations. The
283 first consists a set of 112 randomly selected accessions that have no phenotypic records for
284 PSA and WU. The second consists of a set of 112 accessions that have phenotypic records
285 for PSA, but lack records for WU. Thus, the latter scenario can be thought of as a case
286 where a subset of the population has incomplete data. The predictive ability of MT-RRM1
287 and MT-RRM2 was compared to a ST-RRM in which the model fitted using WU values
288 for 245 accessions and is used to predict genetic values for the remaining 112 accessions. In
289 all cases, the predictive ability was measured as the correlation between predicted genetic
290 values and BLUE in the testing set at each time point.

291 The prediction accuracy for CV1 is shown in Figure 5. An increasing trend in prediction
292 accuracy over time for all models was observed in CV1. Prediction accuracy increased quickly
293 from day 1 to 13, and eventually plateaued from days 14 to 20. MT-RRM2 showed the highest
294 prediction accuracy of all models. On average the predictive ability for MT-RRM2 was 0.74,
295 while for MT-RRM1 and ST-RRM the prediction accuracies were 0.53 and 0.46, respectively.
296 These results indicate that the predictive ability can be improved using a MT-RRM when
297 records for one trait are available for individuals in the testing population. The predictive
298 ability for MT-RRM1 was similar to ST-RRM during the first five time points, but slightly
299 increased with 0.06 to 0.09 relative to ST-RRM from day 6 on ward. These results suggested
300 that MT-RRM approach can be more effective method for genomic prediction of WU.

301 The objective of the second CV scenario was to evaluate the abilities of MT-RRM1 and
302 MT-RRM2 to forecast genetic values at future time points using phenotypes recorded at
303 earlier time points. The design of two MT-RRM were similar to those described above
304 (Figure 1). The first MT-RRM, MT-RRM1, was fit using a training set with WU and PSA
305 data collected from the first 10 time points, and was used to predict genetic values for WU for
306 the subsequent time points. The second MT-RRM, MT-RRM2, was fit using PSA values for
307 all 20 time points and WU values for the first 10 time points, and was used to predict genetic
308 values for WU for the last 10 time points. Figure 6 shows the predictive correlation of WU
309 for each of the models evaluated. The prediction accuracy for each method was relatively
310 constant over all days. However, the prediction accuracy of MT-RRM were greatly higher
311 than ST-RRM, indicating that inclusion of additional information from PSA can improve
312 the ability to forecast WU. For ST-RRM, prediction accuracy ranged from 0.54 to 0.57, while
313 values for MT-RRM1 and MT-RRM2 range from 0.79 to 0.83 and 0.84 to 0.91, respectively.
314 Collectively, these results indicate that joint analysis of PSA and WU with the MT-RRM
315 improves the ability to forecast future genetic values for WU.

316 Discussion

317 Advances in HTP has provided plant breeders with a new suite of tools to assess morphologi-
318 cal and physiological traits in a non-destructive manner for large populations at frequent time
319 intervals throughout the growing season (Fahlgren et al., 2015). These platforms facilitate
320 the collection of data that provide important insights into the morpho-physiological basis of
321 complex traits. Thus, with these technologies complex traits such as drought tolerance can
322 be decomposed into component traits to better understand the basis of these traits and im-
323 prove the development of varieties with increased resilience (Berger et al., 2010). Although
324 these platforms provide a powerful means to quantify complex traits in large populations,
325 some physiological traits require specialized equipment or must be recorded during a specific
326 time of day (e.g., transpiration or chlorophyll fluorescence) (Tardieu et al., 2017). Thus, in
327 many cases these data may only be available for a subset of the population.

328 HTP is often used to record a number of traits on the same individuals. In some cases,
329 physiological traits that are difficult to measure may be correlated with traits that are more
330 accessible and can be recorded with greater ease. In such cases, MT genomic prediction
331 frameworks provide an excellent solution to utilize partial records and predict genetic val-
332 ues for the physiological trait in individuals with missing data. Jia and Jannink (2012)
333 demonstrated that MT models improve prediction accuracy particularly for traits with low
334 heritability. In the current study, we utilized a MT approach in a RRM framework to pre-
335 dict genetic values for WU, a difficult to measure trait with low heritability, by joint analysis
336 with PSA, which exhibits higher heritability and is easier to measure. Since WU shows a
337 positive correlation with PSA, we hypothesized that the MT-RRM framework can improve
338 predictions for WU.

339 Genetic components of HTP image traits

340 Since WU is difficult to quantify directly in cereals such as rice, few studies have measured
341 WU or water use efficiency, while most studies have sought to utilize indirect measurements
342 of WU or water use efficiency for genetic analyses (This et al., 2010; Rebolledo et al., 2013;
343 Feldman et al., 2018; Momen et al., 2019b). Consistent with the current study, Feldman
344 et al. (2018), which utilized a HTP platform to quantify temporal water use and plant size
345 in the C4 species *Setaria* grown in contrasting water regimes, reported moderate broad
346 sense heritability (H^2) values for WU, and higher H^2 for plant size. Moreover, Feldman
347 et al. (2018) showed that H^2 varied throughout the experiment with lower H^2 observed
348 during the initial time points and higher H^2 values observed during the middle time points.
349 In our study, h^2 values for WU in early time points were lower compared to those observed
350 during the later time points. The plants in the current study were relatively small during
351 the initial time points and therefore less amount of water is lost each day. Thus, water
352 loss during these periods may be heavily influenced by environmental factors such as soil
353 temperature or irradiation. Similar temporal trends have been reported for plant height
354 in sorghum (Fernandes et al., 2018). Thus, given the moderate h^2 values for WU and the
355 temporal variability in h^2 , selection for this trait may be difficult in breeding programs.
356 Conversely, h^2 for PSA was relatively stable throughout the experiment, indicating that h^2
357 for PSA may be less affected by temporal environmental effects compared to WU.

358 Multi-trait approaches are particularly advantageous when one target trait has low her-
359 itability and is correlated to a secondary non-target trait with higher heritability (Mrode,
360 2014). Joint analysis using a MT model can improve prediction of genetic values for low her-
361 itability trait and thus improve selection in plant breeding programs. In the current study,
362 we showed a benefit of using MT-RRM for WU which had a positive genomic correlation
363 with PSA. Thus, we proposed that joint analysis of WU with PSA can improve predictions
364 of genetic values for WU. In a recent study, Momen et al. (2019b) examined the relation-
365 ships between single time point measurements of WU, root biomass, water use efficiency,

366 and PSA. According to the result, WU showed a moderate to strong positive correlation
367 with PSA, root biomass, and water use efficiency, ranging from 0.48 to 0.85 (Momen et al.,
368 2019b). Although we utilized PSA as the indicator trait in this study, it is expected that
369 root biomass and water use efficiency can be leveraged for genomic prediction for WU using
370 the MT.

371 **Predictive performance of MT-RRM**

372 The MT-RRM framework offers several advantages over conventional single-trait genomic
373 best linear unbiased prediction (ST-GBLUP) approaches. First, the random regression
374 framework provides a tractable means to predict genetic values for temporal traits. The
375 RRM uses covariances functions to model the genetic and environmental covariance between
376 time points, and has been shown to improve prediction of genetic values compared to a
377 ST-GBLUP approach (Campbell et al., 2018). Secondly, because the covariance function
378 expresses the genetic covariance between time points using a continuous function, the RRM
379 can be used to predict genetic values at time points with no records (Momen et al., 2019a).
380 Thus, we can leverage the RRM framework to forecast future genetic values. Finally, as
381 mentioned above, the joint analysis of MT can improve prediction accuracy for traits with
382 low heritability. In the current study, we designed two CV to evaluate the ability to predict
383 genetic values in unobserved accessions for a trait with lower heritability, and assessed the
384 ability of the MT-RRM to predict future genetic values for accessions with records. Because
385 the sample size and the number of time points used were relatively small, both ST- and
386 MT-RRMs took less than 10 minutes to complete the longitudinal analyses on 64bit Linux
387 with Intel Core i7-6950X (3.0GHz).

388 The first CV scenario was designed to evaluate the ability of MT-RRM to predict ge-
389 netic values for WU in accessions without any records. Consistent with our expectations,
390 MT-RRM had a better predictive ability than ST-RRM. The predictive ability of the MT-

391 RRM was further improved when PSA records were available for accessions in the testing
392 population. The effectiveness of MT genomic models has been investigated extensively and
393 have reported improved prediction accuracy compared to a ST model (Jia and Jannink,
394 2012; Guo et al., 2014; Okeke et al., 2017; Fernandes et al., 2018). For instance, Guo et al.
395 (2014) compared prediction accuracy from ST- and MT-GBLUP using simulated data. MT-
396 GBLUP showed better predictive performance when the target trait had lower heritability
397 compared to the non-target trait and when the target trait had a greater number of missing
398 observations (Guo et al., 2014). However, the majority of these studies have focused on
399 traits recorded at a single time point. In the current study, we used a MT approach for
400 prediction of bivariate traits with longitudinal records, and observed similar results. As sug-
401 gested by the previous studies, an increase of prediction accuracy by MT-RRM in this study
402 may result from a relative lower heritability of WU than PSA and the high degree of shared
403 genetic signals with PSA (Momen et al., 2019b). The results of CV1 showed that prediction
404 accuracies from all the models were more stable at later time periods, which is similar to the
405 temporal trends in prediction accuracy observed for PSA reported by Momen et al. (2019a)
406 that was obtained using a ST-RRM. The accuracy of genomic prediction largely depends
407 on the heritability of the trait (Hayes et al., 2009). Thus, the lower predictions at the ini-
408 tial time points may be the result of the lower heritability observed during these periods.
409 Moreover, early observations are recorded on seedlings that have just started to tiller. At
410 this stage the plants may not have accumulated enough biomass and have low transpiration
411 demands, to discern genotypic variation in water use from environmental variation.

412 Genomic predictions based on small number of records are a major concern in many
413 practical applications, especially for a trait that is difficult or costly to measure because
414 it can reduce phenotyping costs. As expected, the MT approaches (MT-RRM1 and MT-
415 RRM2) in CV2 resulted in improvements compared to the ST-RRM with gains of 0.26 and
416 0.33, on average, for MT-RRM1 and MT-RRM2, respectively. Our results suggest that
417 MT-RRM can be a powerful approach for forecasting future phenotypes using records from

418 earlier periods. In this study, we examined prediction accuracies from 11 to 20 days in CV2.
419 However, the trends in prediction accuracy were relatively stable across time points. Thus,
420 forecasting based on records at further earlier time periods could be implemented without a
421 loss of prediction accuracy as reported by Momen et al. (2019a). However, the performance
422 of these forecasting approaches will likely be highly dependent on the genomic correlation
423 between the time points used to train the prediction model and the time points in which
424 predictions will be made. Lastly, it should be noted that the best prediction performance
425 delivered by MT-RRM2 in both scenarios may be due to the fact that the training-testing
426 sets partitioning is not completely independent in a strict sense. However, a situation akin
427 to this occurs in practice and an approach such as MT-RRM2 would be still worthwhile to
428 test.

429 We employed an unweighted two-stage approach to obtain adjusted means because of its
430 simplicity and computational efficiency. However, a single-stage analysis is often considered
431 as a more appropriate method to account for systematic effects due to heterogeneity of
432 covariances among adjusted means (Möhring and Piepho, 2009; Piepho et al., 2012). Thus,
433 we also explored a single-stage analysis by fitting all the systematic effects in RRM. We
434 observed a high correlation (0.92) between the genetic values from the single-stage and the
435 unweighted two-stage analyses across 20 time points. This is likely because the current
436 dataset is obtained from the control condition in a greenhouse, which may yield a more
437 homogeneous variance-covariance structure of errors between adjusted means compared to
438 heterogeneous data typically collected from multi environment field trials. A weighted two-
439 stage approach (Smith et al., 2001; Piepho et al., 2012) was not considered in the current
440 study because of the limitation of the GIBBS3F90 program to perform such an analysis.

441 **Conclusion**

442 To our knowledge, this is the first study that applied the MT-RRM to HTP-derived temporal
443 traits in plants. We demonstrated that MT-RRM is a robust and flexible approach that can
444 be used to improve prediction accuracy for a trait with a limited number of records or low
445 heritability. Thus, in the case of breeding for morpho-physiological traits, the MT-RRM can
446 improve prediction accuracy for physiological traits that may have low heritability or are
447 difficult to measure in large populations.

448 **Acknowledgments**

449 This work was supported by the National Science Foundation under Grant Number 1736192
450 to HW and GM, and Virginia Polytechnic Institute and State University startup funds to
451 GM.

452 **Author contribution statement**

453 This work was supported by the National Science Foundation under Grant Number 1736192
454 to HW and GM, and Virginia Polytechnic Institute and State University startup funds to
455 GM. MTC and HW designed and conducted the experiments. TB and MM analyzed the
456 data. TB and GM conceived the idea and wrote the manuscript. MTC, MM and HW
457 discussed results and revised the manuscript. GM supervised and directed the study. All
458 authors read and approved the manuscript.

459 Figures

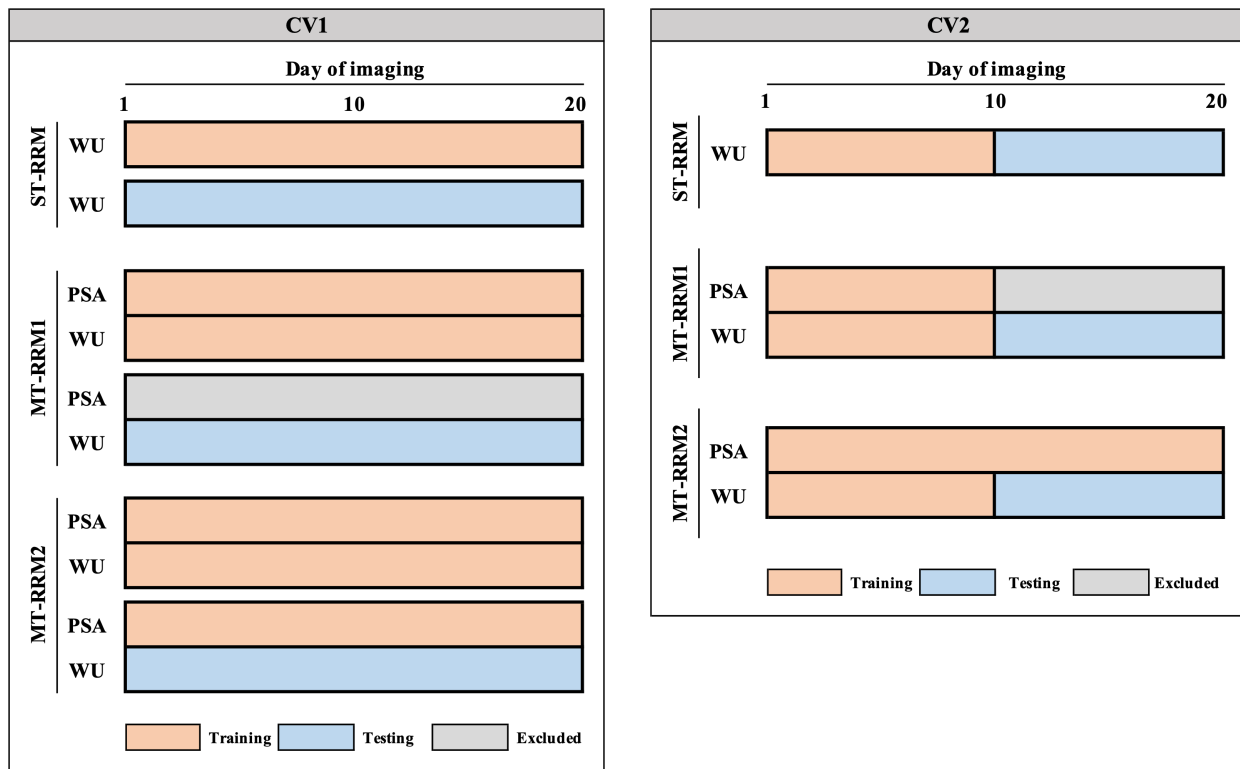


Figure 1: Two scenarios of cross-validation (CV) designed to investigate prediction accuracy of water use (WU) from single- and multi-trait random regression models (ST-RRM, MT-RRM1, and MT-RRM2). CV1: Prediction of WU for a set of 112 accessions without records on WU using 245 training accessions. ST-RRM: single-trait random regression model using WU of training accessions; MT-RRM1: multi-trait random regression model using WU and projected shoot area (PSA) of training accessions; MT-RRM2: multi-trait random regression model using WU and PSA of training accessions as well as PSA of testing accessions. CV2: Forecast future genetic values of WU belonging to 245 known accessions from records at earlier time periods. ST-RRM: single-trait random regression model for WU using the first 10 time points in training accessions; MT-RRM1: multi-trait random regression model for WU using the first 10 time points of WU and PSA information in training accessions; MT-RRM2: multi-trait random regression model for WU using WU from 1 to 10 time periods and PSA at all the time periods in training accessions.

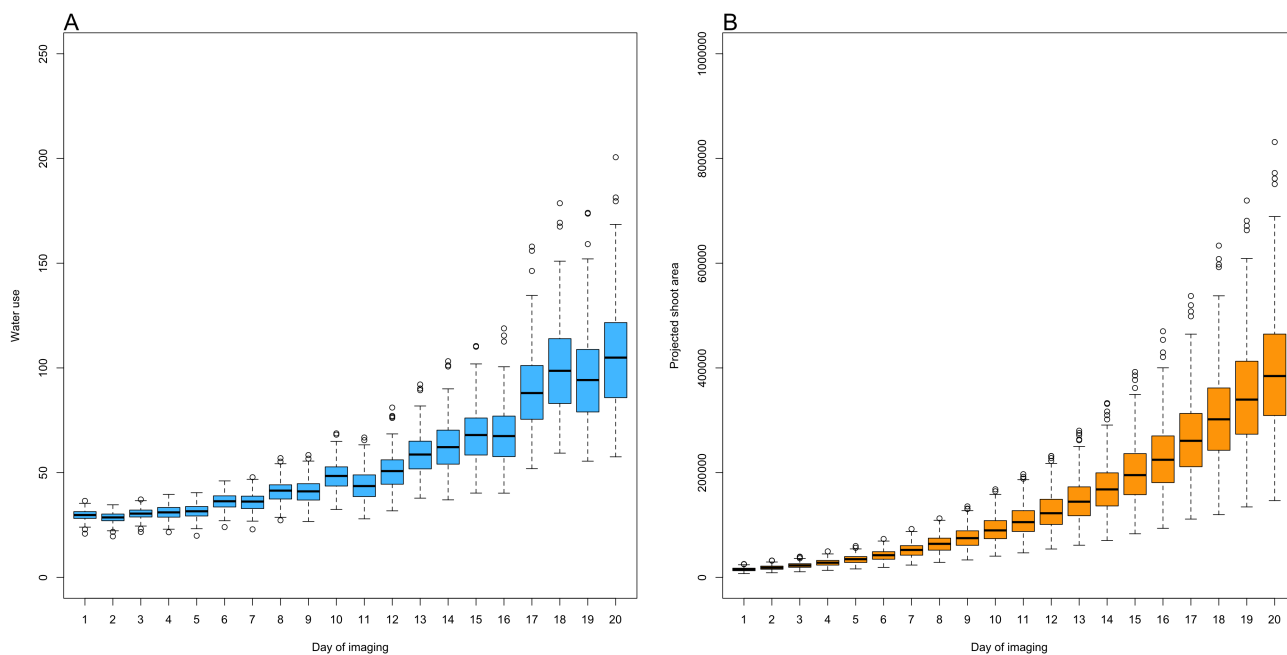


Figure 2: A boxplot of best linear unbiased estimator for water use (A) and projected shoot area (B) over 20 days of imaging.

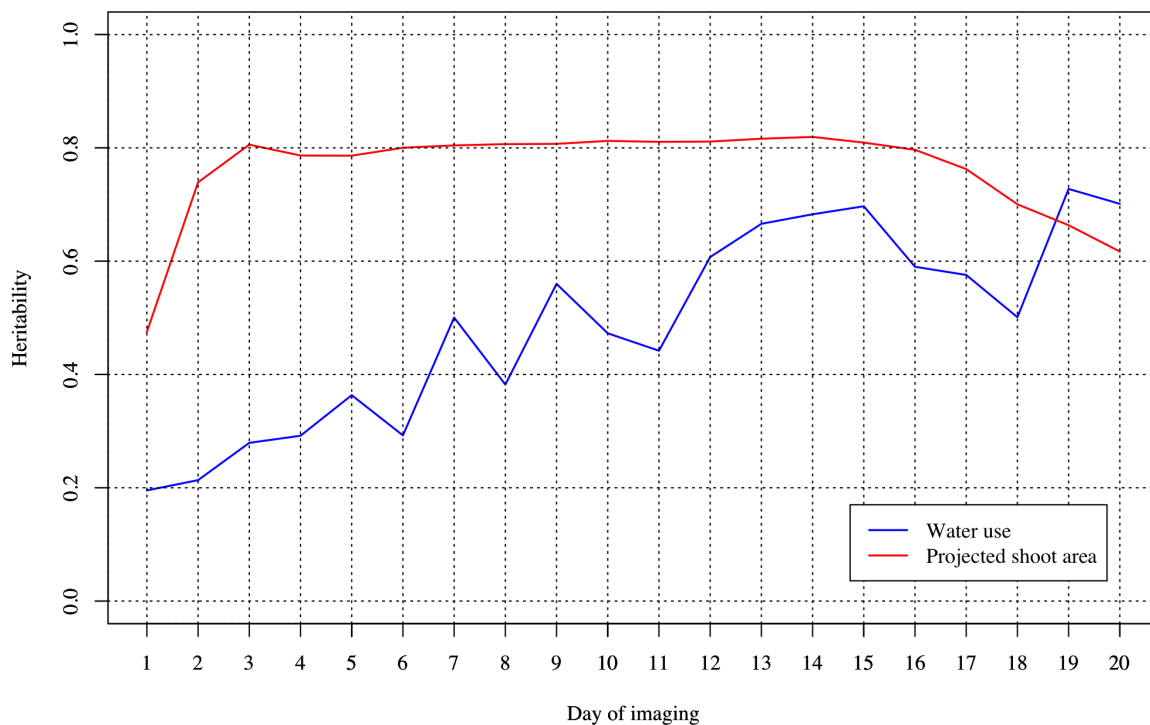


Figure 3: Heritability for water use and projected shoot area over 20 days of imaging using a single-trait random regression model.

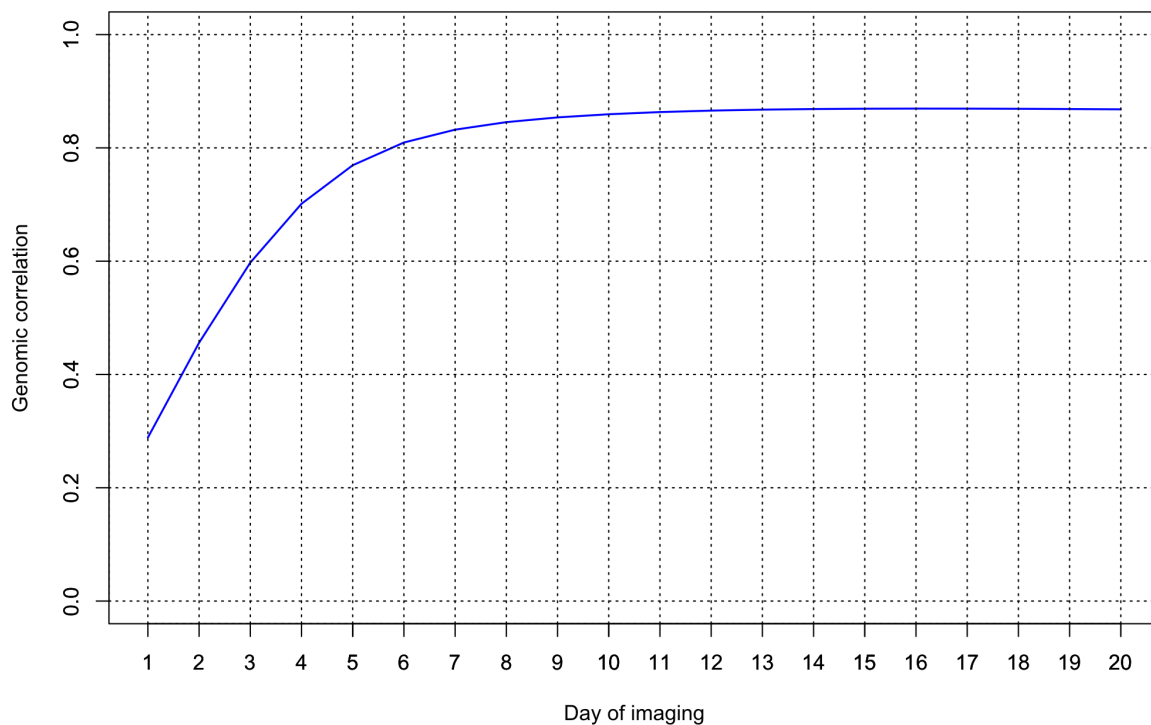


Figure 4: Genomic correlation between water use and projected shoot area over 20 days of imaging using a multi-trait random regression model.

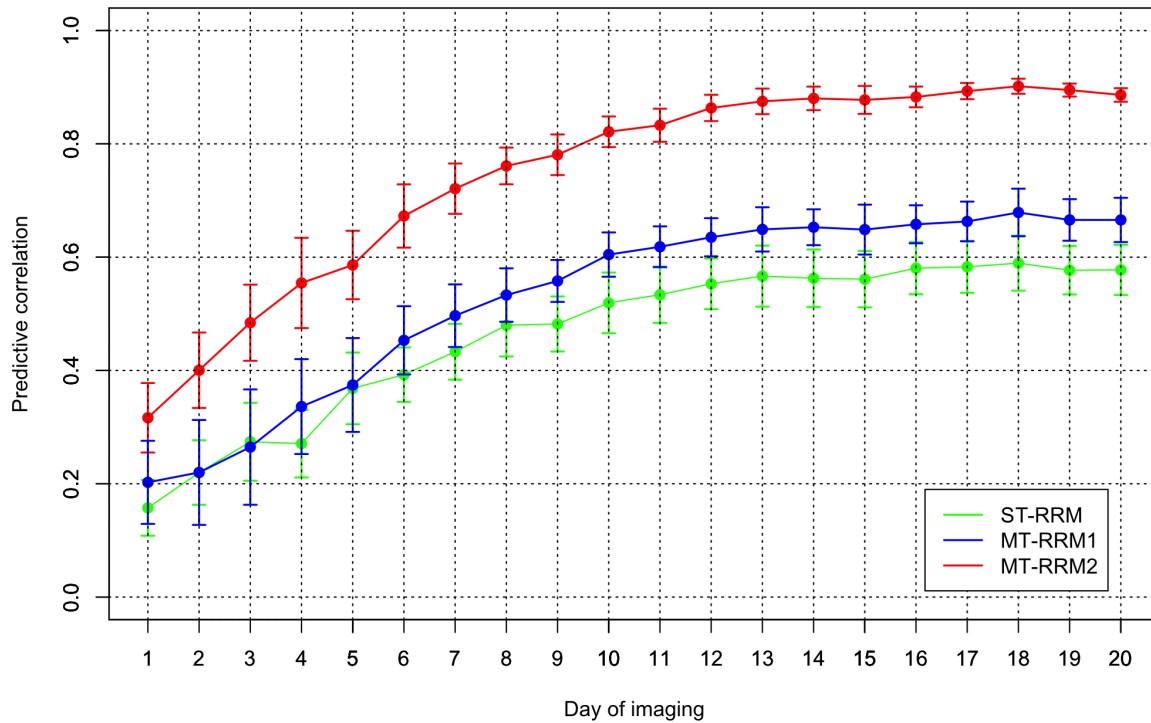


Figure 5: Pearson correlation of water use from cross-validation scenario 1. ST-RRM: single-trait random regression model; MT-RRM1: multi-trait random regression model using the water use and projected shoot area of training data; MT-RRM2: multi-trait random regression model using the water use and projected shoot area of training data as well as the PSA of testing data.

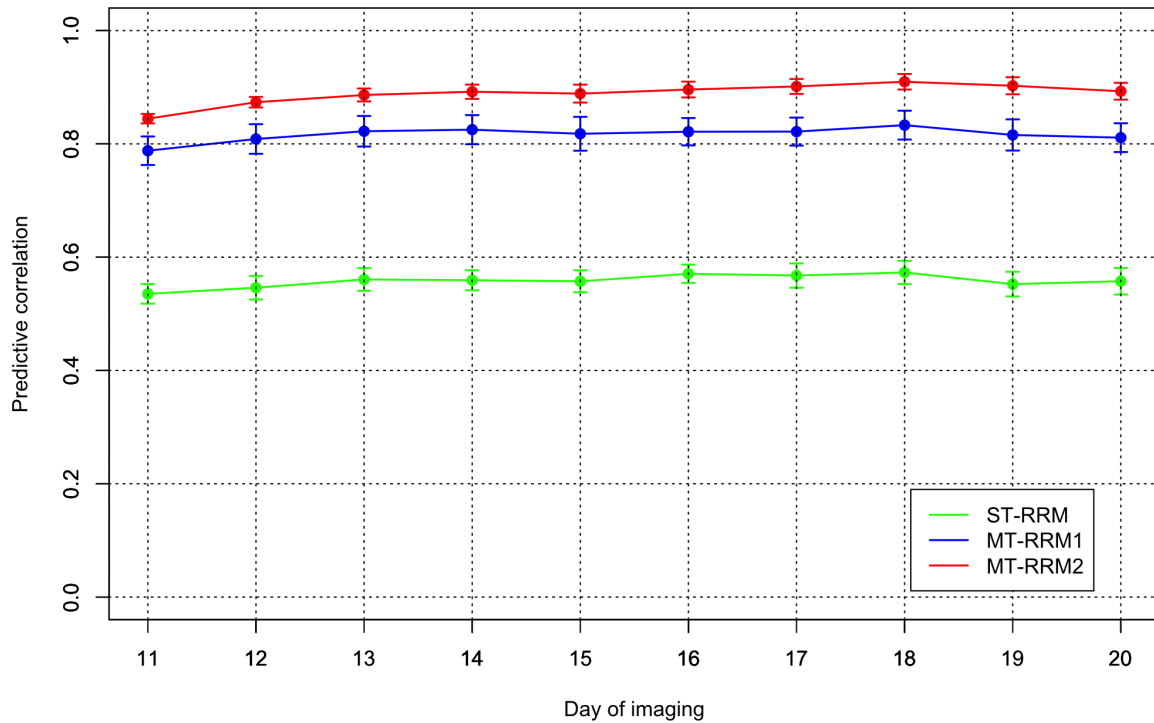


Figure 6: Pearson correlation of water use from cross-validation scenario 2. ST-RRM: single-trait random regression model; MT-RRM1: multi-trait random regression model using WU and PSA from 1 to 10 time periods in the training data; MT-RRM2: multi-trait random regression model using WU from 1 to 10 time periods and PSA at all the time periods in the training data.

460 References

- 461 Araus, J. L., Kefauver, S. C., Zaman-Allah, M., Olsen, M. S., and Cairns, J. E. (2018).
462 Translating high-throughput phenotyping into genetic gain. *Trends in Plant Science*,
463 23(5):451–466.
- 464 Berger, B., Parent, B., and Tester, M. (2010). High-throughput shoot imaging to study
465 drought responses. *Journal of Experimental Botany*, 61(13):3519–3528.
- 466 Browning, S. R. and Browning, B. L. (2007). Rapid and accurate haplotype phasing and
467 missing-data inference for whole-genome association studies by use of localized haplotype
468 clustering. *The American Journal of Human Genetics*, 81(5):1084–1097.
- 469 Calus, M. P. and Veerkamp, R. F. (2011). Accuracy of multi-trait genomic selection using
470 different methods. *Genetics Selection Evolution*, 43(1):26.
- 471 Campbell, M., Momen, M., Walia, H., and Morota, G. (2019). Leveraging breeding values
472 obtained from random regression models for genetic inference of longitudinal traits. *The*
473 *Plant Genome*.
- 474 Campbell, M., Walia, H., and Morota, G. (2018). Utilizing random regression models for ge-
475 nomic prediction of a longitudinal trait derived from high-throughput phenotyping. *Plant*
476 *Direct*, 2(9):e00080.
- 477 Campbell, M. T., Knecht, A. C., Berger, B., Brien, C. J., Wang, D., and Walia, H. (2015).
478 Integrating image-based phenomics and association analysis to dissect the genetic archi-
479 tecture of temporal salinity responses in rice. *Plant Physiology*, 168(4):1476–1489.
- 480 Cullis, B. R., Smith, A. B., and Coombes, N. E. (2006). On the design of early generation
481 variety trials with correlated data. *Journal of Agricultural, Biological, and Environmental*
482 *Statistics*, 11(4):381.

- 483 Fahlgren, N., Gehan, M. A., and Baxter, I. (2015). Lights, camera, action: high-throughput
484 plant phenotyping is ready for a close-up. *Current Ppinion in Plant Biology*, 24:93–99.
- 485 Feldman, M. J., Ellsworth, P. Z., Fahlgren, N., Gehan, M. A., Cousins, A. B., and Baxter,
486 I. (2018). Components of water use efficiency have unique genetic signatures in the model
487 c4 grass setaria. *Plant Physiology*, 178(2):699–715.
- 488 Fernandes, S. B., Dias, K. O., Ferreira, D. F., and Brown, P. J. (2018). Efficiency of multi-
489 trait, indirect, and trait-assisted genomic selection for improvement of biomass sorghum.
490 *Theoretical and Applied Genetics*, 131(3):747–755.
- 491 Gengler, N., Tijani, A., Wiggans, G., and Misztal, I. (1999). Estimation of (co) variance func-
492 tion coefficients for test day yield with a expectation-maximization restricted maximum
493 likelihood algorithm. *Journal of Dairy Science*, 82(8):1849–e1.
- 494 Golzarian, M. R., Frick, R. A., Rajendran, K., Berger, B., Roy, S., Tester, M., and Lun,
495 D. S. (2011). Accurate inference of shoot biomass from high-throughput images of cereal
496 plants. *Plant Methods*, 7(1):2.
- 497 Guo, G., Zhao, F., Wang, Y., Zhang, Y., Du, L., and Su, G. (2014). Comparison of single-
498 trait and multiple-trait genomic prediction models. *BMC Genetics*, 15(1):30.
- 499 Hayes, B. J., Bowman, P. J., Chamberlain, A., and Goddard, M. (2009). Invited review:
500 Genomic selection in dairy cattle: Progress and challenges. *Journal of Dairy Science*,
501 92(2):433–443.
- 502 Jia, Y. and Jannink, J.-L. (2012). Multiple-trait genomic selection methods increase genetic
503 value prediction accuracy. *Genetics*, 192(4):1513–1522.
- 504 Juliana, P., Montesinos-López, O. A., Crossa, J., Mondal, S., Pérez, L. G., Poland, J.,
505 Huerta-Espino, J., Crespo-Herrera, L., Govindan, V., Dreisigacker, S., et al. (2019). In-

- 506 tegrating genomic-enabled prediction and high-throughput phenotyping in breeding for
507 climate-resilient bread wheat. *Theoretical and Applied Genetics*, 132(1):177–194.
- 508 Kadarmideen, H. N., Thompson, R., Coffey, M. P., and Kossaibati, M. A. (2003). Genetic
509 parameters and evaluations from single-and multiple-trait analysis of dairy cow fertility
510 and milk production. *Livestock Production Science*, 81(2-3):183–195.
- 511 Kirkpatrick, M., Lofsvold, D., and Bulmer, M. (1990). Analysis of the inheritance, selection
512 and evolution of growth trajectories. *Genetics*, 124(4):979–993.
- 513 Knecht, A. C., Campbell, M. T., Caprez, A., Swanson, D. R., and Walia, H. (2016). Image
514 Harvest: an open-source platform for high-throughput plant image processing and analysis.
515 *Journal of Experimental Botany*, 67(11):3587–3599.
- 516 Meyer, K. and Hill, W. G. (1997). Estimation of genetic and phenotypic covariance functions
517 for longitudinal or repeated records by restricted maximum likelihood. *Livestock Production
518 Science*, 47(3):185–200.
- 519 Misztal, I., Tsuruta, S., Strabel, T., Auvray, B., Druet, T., Lee, D., et al. (2002). Blupf90
520 and related programs (bglf90). In *Proceedings of the 7th world congress on genetics applied
521 to livestock production*, volume 33, pages 743–744.
- 522 Möhring, J. and Piepho, H.-P. (2009). Comparison of weighting in two-stage analysis of
523 plant breeding trials. *Crop Science*, 49(6):1977–1988.
- 524 Momen, M., Campbell, M. T., Walia, H., and Morota, G. (2019a). Predicting longitudinal
525 traits derived from high-throughput phenomics in contrasting environments using genomic
526 legendre polynomials and b-splines. *G3: Genes, Genomes, Genetics*, page In press.
- 527 Momen, M., Campbell, M. T., Walia, H., and Morota, G. (2019b). Utilizing trait networks
528 and structural equation models as tools to interpret multi-trait genome-wide association
529 studies. *bioRxiv*, page 553008.

- 530 Morota, G., Jarquin, D., Campbell, M. T., and Iwata, H. (2019). Statistical methods for
531 the quantitative genetic analysis of high-throughput phenotyping data. *arXiv preprint*
532 *arXiv:1904.12341*.
- 533 Mrode, R. A. (2014). *Linear models for the prediction of animal breeding values*. Cabi.
- 534 Okeke, U. G., Akdemir, D., Rabbi, I., Kulakow, P., and Jannink, J.-L. (2017). Accuracies
535 of univariate and multivariate genomic prediction models in african cassava. *Genetics*
536 *Selection Evolution*, 49(1):88.
- 537 Piepho, H.-P., Moehring, J., Schulz-Streeck, T., and Ogutu, J. O. (2012). A stage-wise
538 approach for the analysis of multi-environment trials. *Biometrical Journal*, 54(6):844–860.
- 539 Rebolledo, M. C., Luquet, D., Courtois, B., Henry, A., Soulié, J.-C., Rouan, L., and
540 Dingkuhn, M. (2013). Can early vigour occur in combination with drought tolerance
541 and efficient water use in rice genotypes? *Functional Plant Biology*, 40(6):582–594.
- 542 Schaeffer, L. (2004). Application of random regression models in animal breeding. *Livestock*
543 *Production Science*, 86(1-3):35–45.
- 544 Schaeffer, L. and Dekkers, J. (1994). Random regressions in animal models for test-day
545 production in dairy cattle. In *World Congress of Genetics Applied Livestock Production,*
546 *1994*, volume 18, pages 443–446.
- 547 Smith, A., Cullis, B., and Gilmour, A. (2001). Applications: the analysis of crop variety
548 evaluation data in australia. *Australian & New Zealand Journal of Statistics*, 43(2):129–
549 145.
- 550 Sun, J., Rutkoski, J. E., Poland, J. A., Crossa, J., Jannink, J.-L., and Sorrells, M. E.
551 (2017). Multitrait, random regression, or simple repeatability model in high-throughput
552 phenotyping data improve genomic prediction for wheat grain yield. *The Plant Genome*.

- 553 Tardieu, F., Cabrera-Bosquet, L., Pridmore, T., and Bennett, M. (2017). Plant phenomics,
554 from sensors to knowledge. *Current Biology*, 27(15):R770–R783.
- 555 This, D., Comstock, J., Courtois, B., Xu, Y., Ahmadi, N., Vonhof, W. M., Fleet, C., Setter,
556 T., and McCouch, S. (2010). Genetic analysis of water use efficiency in rice (*oryza sativa*
557 l.) at the leaf level. *Rice*, 3(1):72.
- 558 VanRaden, P. M. (2008). Efficient methods to compute genomic predictions. *Journal of*
559 *Dairy Science*, 91(11):4414–4423.
- 560 Voss-Fels, K. P., Cooper, M., and Hayes, B. J. (2019). Accelerating crop genetic gains with
561 genomic selection. *Theoretical and Applied Genetics*, 132(3):669–686.
- 562 Zhao, K., Tung, C.-W., Eizenga, G. C., Wright, M. H., Ali, M. L., Price, A. H., Norton,
563 G. J., Islam, M. R., Reynolds, A., Mezey, J., et al. (2011). Genome-wide association
564 mapping reveals a rich genetic architecture of complex traits in *oryza sativa*. *Nature*
565 *Communications*, 2:467.